AIP | Review of Scientific Instruments

Space charge lenses for particle beams

J. Pozimski and O. Meusel

Citation: Review of Scientific Instruments **76**, 063308 (2005); doi: 10.1063/1.1904203
View online: http://dx.doi.org/10.1063/1.1904203
View Table of Contents: http://scitation.aip.org/content/aip/journal/rsi/76/6?ver=pdfcov
Published by the AIP Publishing

Space charge lenses for particle beams

J. Pozimski[a] and O. Meusel
Institut für Angewandte Physik der Johann Wolfgang Goethe Universität, Robert-Mayer-Strasse 2-4, D-60054 Frankfurt am Main, Germany

(Received 16 July 2004; accepted 17 February 2005; published online 1 June 2005)

Space charge lenses provide strong cylinder symmetric focusing for low-energy high-perveance particle beams using a stable space charge cloud. They need drastically reduced magnetic and electrostatic field strength compared with conventional systems and are superior for a degree of lens filling above 17%. They can theoretically provide linear transformation in phase space and reduce beam aberrations and space charge forces. The density distribution of the enclosed space charge is given by the transverse and longitudinal enclosures of the cloud. By the use of self-consistent simulations of the space charge cloud, the focusing properties of space charge lenses in the presented design can be forecasted with sufficient quality. The presented simulations show that the theoretical values can be reached locally. The results of our investigations on the beam transport in a high-current test injector equipped with space charge lenses, including emittance measurements, will be presented and discussed. They show that significant improvements of lens operation have been reached by the reduction of the residual gas pressure and a careful design of the external fields using numerical simulation techniques to calculate the local density distributions. Comparisons of the experimental results with the beam transport simulations show good agreement concerning both focusing strength and linearity of phase space transformation. For the lens design used, the observed degree of lens filling is at least 38% of the theoretical value and more than twice the threshold value. © *2005 American Institute of Physics*. [DOI: 10.1063/1.1904203]

I. INTRODUCTION

Space charge fields for the focusing of particle beams have already been considered in the early 20th century. Westphal and Johnson observed self-focusing of channel rays within a residual gas atmosphere.[1,2] Further considerations on space charge focusing and the experimental use of these effects within a specially designed lens device to focus particle beams have been published by Borries and Ruska.[3] Gabor published the first suggestion for a space charge lens using magnetic fields for space charge confinement.[4] For such a device, he described theoretically the limit for the radial charge density within the lens using the theory on the electron confinement within magnetic fields published by Brillouin.[5] The theoretical performance of space charge lenses is, compared with conventional lens systems, very advantageous. Only space charge fields can theoretically provide a strong linear cylinder symmetric force on the beam particles and hence a linear transformation in the transversal phase space. For focusing low-energy ion beams (especially for heavy ion inertial fusion)[6] the use of a magnetically confined electron cloud could reduce the required external fields by a factor of 10 and could simultaneously reduce emittance growth by external field errors and space charge forces of the ion beam. These features are the reason for the ongoing theoretical and experimental work on space charge lenses, which has been published by different workgroups.[7–10] On the other hand, the unsatisfactory experimental results reported for such lenses concerning space charge density and beam aberrations caused by inhomogeneous lens filling have impeded the practical use so far.

II. THEORY

Let us assume a space charge lens similar to the suggestion of Gabor. The space charge cloud is confined longitudinally by the potential of a central cylindrical anode surrounded by two grounded electrodes and radially by a magnetic solenoidal field. Assuming Brillouin flow, the maximum density n_r of the space charge particles with mass m is defined by the radial enclosure condition and is given by

$$n_r = \frac{\varepsilon_0}{2m} B^2. \tag{1}$$

On the other hand, for the longitudinal enclosure by the anode potential, the maximum particle density n_l can be derived by assuming an homogeneous filled cylinder with a radius r_A of the anode and a potential depression of V_A using

$$n_l = \frac{4\varepsilon_0 V_A}{e r_A^2}. \tag{2}$$

This is valid for electrons produced within the lens. For electrons starting on ground potential, as proposed by Gabor, the maximum density is reached for the space charge potential $V_{SC}=(2/3)V_A$. The maximum space charge particle density given by the minimum of both relations (1) and (2) is shown in Fig. 1.

[a]Electronic mail: juergen@pozimski.de

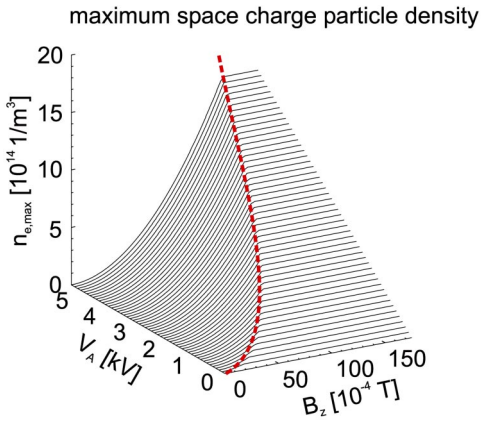

FIG. 1. (Color online) Space charge density according to the longitudinal and radial enclosures.

If both equations are fulfilled simultaneously ($n_r = n_l$; dotted in Fig. 1), the voltage on the anode is then given by the magnetic field and the anode radius, as

$$V_A = \frac{e r_A^2 B^2}{8m}. \tag{3}$$

For the determination of the space charge density within a lens by theory, several difficulties occur. Where for the radial confinement external electric fields are neglected (condition A, Fig. 2), for the longitudinal confinement the radius of the space charge cloud is set to be the anode radius. Additional effects associated with the interactions of the trapped electrons, such as charge production, thermalization of the space charge ensemble, and diffusion of particles across magnetic field lines (condition C, Fig. 2) are also neglected. Therefore, no sufficient theory to describe the focusing characteristics of space charge lenses is available.

To compare the experimental results gained by different lenses and to characterize the trapping efficiency, the parameter κ ($0 < \kappa < 1$) is defined as

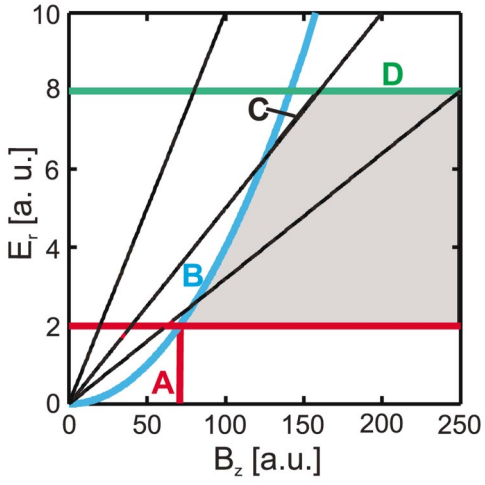

FIG. 2. (Color online) The radial space charge field within the lens as a function of the magnetic field is limited by four border conditions. A: minimum electric field without electrons, B: Brillouin flow limit, C: radial diffusion across magnetic field lines, and D: longitudinal enclosure.

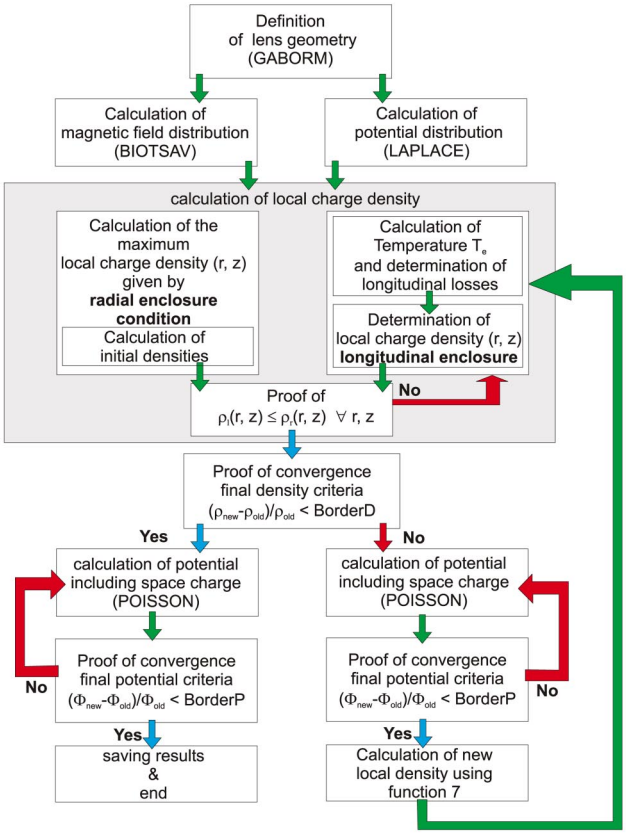

FIG. 3. (Color online) Schematic flow diagram of the iterative simulation process for the self-consistent calculation of space charge densities.

$$\kappa_r = \frac{n_{\exp}}{n_r} \tag{4}$$

radially, and longitudinally, as

$$\kappa_l = \frac{n_{\exp}}{n_l}. \tag{5}$$

Previous experiments have shown κ smaller than 0.07. For the transport of particle beams, the use of space charge lenses is advantageous for κ greater than 0.17 using internal filling and $\kappa > 0.26$ for external electrons.[11]

III. NUMERICAL SIMULATIONS

For a detailed analysis of the space charge distribution within an experimental setup, and to compare the results with the experimental data, a numerical simulation using a two-dimensional grid was developed. For each grid point, the local radial electric field strength given by

$$E_{r,B}(r,z) = \frac{e}{4m} B_z^2(r,z) r \tag{6}$$

is calculated and compared with the existing electric field $E(r)$ generated by the space charge density and the Laplace boundary conditions. Using the difference between those electric field values, a new local space charge density can be derived using

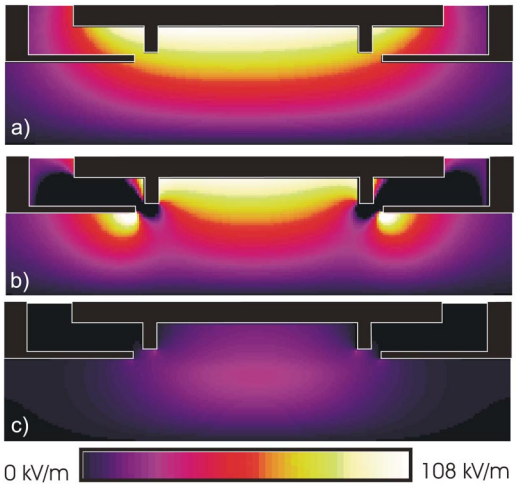

FIG. 4. (Color online) Radial electric field as a function of r and z.

$$\rho_{r,\mathrm{new}}(r,z) = \rho_{r,\mathrm{old}}(r,z) + \Gamma\left\{\frac{2\varepsilon_0[E_{r,B}(r,z) - E_r(r,z)]}{r}\right\}. \tag{7}$$

A numerical relaxation factor Γ $(0<\Gamma<1)$ is used to avoid an overestimation of the local charge density and to improve convergence. To couple these local space charge densities calculated from the radial enclosure conditions longitudinally, a thermalization of the space charge cloud along magnetic field lines is assumed. Using a Boltzmann distribution for the calculation of the longitudinal enclosure,

$$\rho_l[\phi(r_{n1},z_{m1})] = \rho_r[\phi_{\max}(r_{n2},z_{m2})]e^{[\phi_{\max}(r_{n2},zm_2)-\phi(r_{n1},z_{n1})/kT]},$$

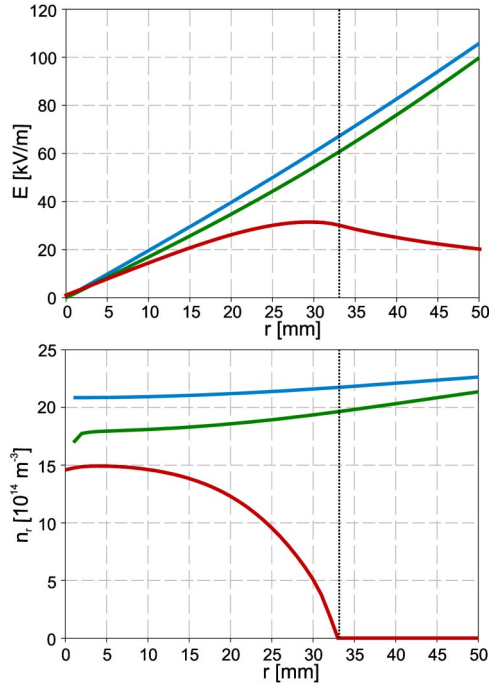

FIG. 5. (Color online) Radial electric field (upper plot) and space charge density lower plot) as a function of the radius at the center of the lens (blue: radial enclosure, green: external electric field, red: contribution of space charge).

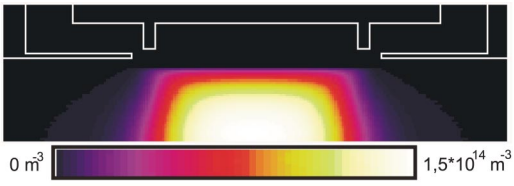

FIG. 6. (Color online) Space charge density distribution as a function of r and z. In the center of the lens the space charge density reaches 70% of the theoretical value.

$$\forall B(n1,m1) = B(n2,m2), \tag{8}$$

an electron temperature has to be assumed. Therefore, the total current I_l produced by longitudinal losses of space charge particles, can be calculated by the integral on the loss current density $j(r)$, as

$$I_l = \int_0^r j(r) r dr. \tag{9}$$

The loss current density is then given by the charge density at ground potential $\rho(\Phi=0)$ and the average particle velocity $\bar{v}$:

$$j(r) = \rho(\Phi = 0)\bar{v}. \tag{10}$$

For simplification, the following approximation

$$j(r) = \rho(\Phi_{\max})e^{-(\Phi_{\max}/kT)}\sqrt{\frac{ekT}{m}} \tag{11}$$

is used to numerically calculate the upper loss current density. The simulation calculates the electron temperature T for a given longitudinal loss current I_l assuming a constant current density $j(r)$. The derived longitudinal charge densities have additionally to fulfill the relation $\rho_l(r,z) \leqslant \rho_r(r,z)$ everywhere, otherwise the temperature is adjusted to be suitable. The code generates the self-consistent density distribution of the space charge cloud in an iterative way using the numerical damping factor Γ to reach convergence, as shown in Fig. 3. For a given geometry of the external magnetic and electric fields, the density distribution of the space charge cloud is only a function of the production mechanisms and can be summarized in the loss current I_l.

According to the experimental data for low residual gas pressure in the lens $(1\times10^{-6}$ hPa), typical values of I_l are in the range of $1-100$ μA. For the presented geometry of 12 960 mesh points and using a damping factor Γ of 0.6 numerical convergence can be reached within 100 to 500 cycles.

For the presented results of the simulations, a field configuration according to the experimental setup was used.

In Fig. 4, three different electric field distributions $[\mathrm{A}:E_{r,B}(r,z),\mathrm{B}:E_{r,B}(r,z)-E_r,\mathrm{C}:E_{r,p}(r,z)]$ are shown. The electric field due to the theory of radial enclosure (plot a), shows an increase towards the magnetic field coils. In plot (b), the reduction of those space charge fields by the external electric field is shown. The external fields additionally prevent space charge densities between the electrodes. The gained space charge field (plot c) is again smaller than predicted by the radial enclosure condition.

In Fig. 5, the electric field (upper plot) and the space

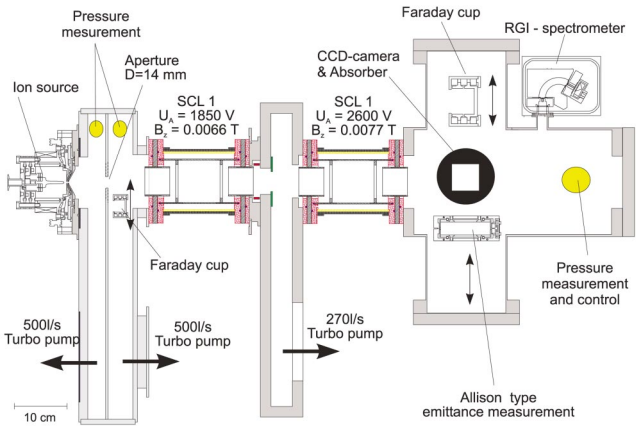

FIG. 7. (Color online) Schematic drawing of the experimental setup used for the measurements of beam transport by the use of plasma lenses.

charge particle density (lower plot) as a function of the radius at the center of the lens is shown. Within 20 mm, the electric field of the space charge is nearly linear. Near the lens axis, space charge density reaches up to 70% of the theoretical value. For radii larger than 20 mm, the space charge density is strongly reduced, and it vanishes above 30 mm.

In Fig. 6, the space charge particle density as a function of r and z is plotted. Where in the center of the lens the theoretical density is nearly reached ($\sim$70%), the strong influence of the electrodes on the longitudinal and radial elongation of the cloud is clearly visible.

IV. EXPERIMENTAL SETUP

The experimental setup used for the presented beam transport experiments is shown in Fig. 7. A thermal cathode driven gas discharge in a volume type ion source produces a dc ion beam of $\sim$9 mA of helium with a beam energy of

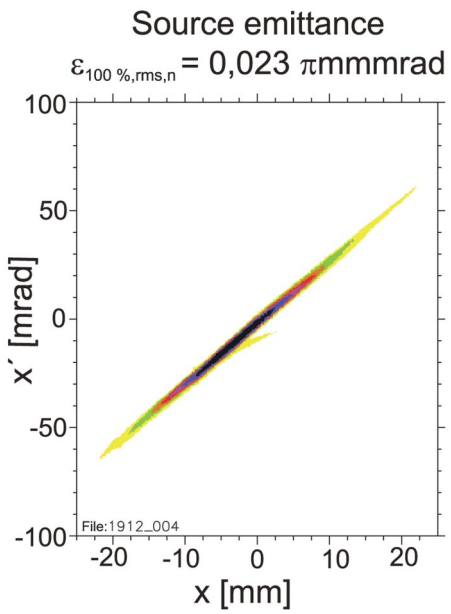

FIG. 8. (Color online) Transversal beam emittance (x,x') measured between the ion source and the first lens.

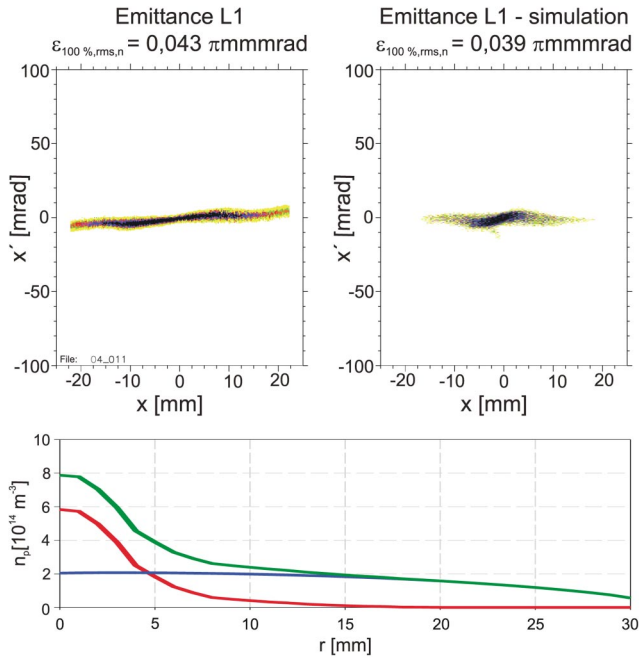

FIG. 9. (Color online) Transversal beam emittance (x,x') measured at the end of the LEBT. Only the first lens is operational. Left: measured phase space density, right: result of simulation. Lower plot: Radial particle density in the center of the first lens (red: beam ions, green: electrons, blue: net particle density).

14 keV. A differential pumping stage to reduce the residual gas pressure in the low energy beam transport (LEBT) is installed behind the ion source. Two identical space charge lenses separated by an additional pumping and diagnostics chamber focus the beam into the final diagnostic chamber. The beam transport for the chosen beam energy and current is strongly dominated by space charge forces. The influence of space charge forces on the beam characterized by the generalized perveance $K(K=0.08)$ is even higher than for the IFMIF ($K=0.04$) or HIDIF ($K=0.06$) projects and demonstrates the special ability of space charge lenses for high-current accelerators. Measurements of the beam current by the use of Faraday cups and emittance measurements using an Allison scanner device can be performed along the beam axis. Additionally, a CCD camera monitors the beam, and the degree of space charge compensation is determined by the use of a residual gas ion energy spectrometer of the Hughes-Ranjovsky type. For the experiments, the residual gas pressure was on the order of 3×10^{-6} hPa and dominated by the gas flow from the ion source. The beam current was 8.6 mA and the beam transmission through the LEBT above 95%.

V. EXPERIMENTAL RESULTS

To compare the experimental results of the beam transport measurements with the results of the beam transport and space charge simulations, the normalized phase space density in the transversal x,x'-plane ($\varepsilon_{100\%,\mathrm{RMS},n}$) is used. In Fig. 8, the phase space density measured at LEBT entrance is shown.

The initial phase space density distribution for the beam transport calculations was taken from this measurement.

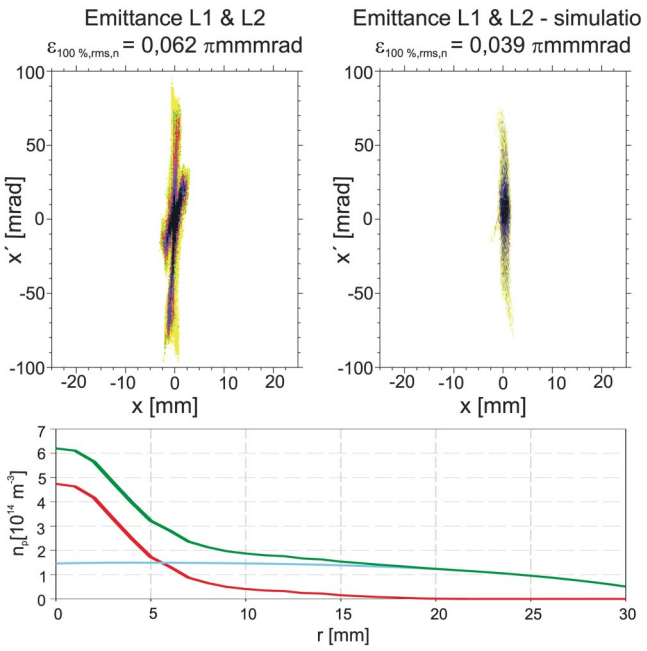

FIG. 10. (Color online) Transversal beam emittance (x,x') measured at the end of the LEBT. Both lenses are operational. Left: measured phase space density, right: result of simulation. Lower plot: Radial particle density in the center of the second lens (red: beam ions, green: electrons, blue: net particle density).

Therefore, an ensemble of 10 000 macroparticles represents the beam, and the transport is calculated including the focusing fields determined by the space charge simulations using the code LINTRA.[12] A degree of space charge compensation of 95% outside the lenses and 100% inside was assumed for the calculations.

In the first experiment, only the first lens was operational and was adjusted to form a parallel beam. The lens parameters where $B_z=6.6\times10^{-3}$ T for the confining magnetic field and an anode voltage of $U_A=1.85$ kV.

In Fig. 9, the measured phase space density is shown (upper left plot). The observed emittance growth is 0.02 π mm mrad for the first lens including the drift sections. The results of the beam transport simulation are presented on the upper right plot. The calculated phase space distribution is very similar to the measured one as well as the predicted emittance growth. Both show, for the presented lens parameters, a variation of the envelope angle of the ion beam of 60 mrad. In the lower plot, the radial particle density distribution in the center of the lens is shown. For a beam radius of 12 mm within the lens (red line) the resolving space charge density is nearly homogeneous, with a variation of ±1.5%. In the second experiment, the parameters of the first lens were kept constant and the second lens was adjusted to form a focus at the Allison emittance scanner device. The parameters of the second lens were $B_z=7.7\times10^{-3}$ T for the confining magnetic field and an anode voltage of $U_A=2.6$ kV.

In Fig. 10, the measured phase space density is shown (upper left plot). In this experiment, an additional variation of the envelope angle of the ion beam of 100 mrad has been observed. In this case, an emittance growth of 0.019 π mm mrad was observed. These values of emittance growth are comparable with conventional lens systems like solenoids or einzellenses for space charge dominated beam transport. For a solenoid LEBT, using similar beam parameters, an emittance growth of 0.056 π mm mrad (for both lenses together) was measured in our laboratory. The calculated phase space distribution (right plot) is still very similar to the measured one. On the other hand, in this experiment the predicted emittance growth is much smaller than the measured value. For a beam radius of 12 mm within the lens, as shown in the lower plot, the space charge density is nearly homogeneous, with a variation of ±2.6%. As a result beam aberrations caused by nonlinear focusing fields in the lenses are nearly negligible for beam radii smaller than 15 mm. For higher beam radii, the decreasing space charge density causes strong nonlinear effects. The results of beam transport simulations show good agreement of the orientation of the phase space density distribution compared with measurements. The quality of the beam emittance growth forecast by the simulations has not reached this level so far.

TABLE I. Comparison of space charge particle densities gained by theory, simulation, and measurements for the first experiment.

Lens 1	$n_{e,\max}[\mathrm{m}^{-3}]$	$\bar{n}_e[\mathrm{m}^{-3}]$
Radial enclosure	2.1×10^{14}	2.1×10^{14}
Longitudinal enclosure	1.6×10^{14}	1.6×10^{14}
Simulation	1.5×10^{14} (71%/93%)	1.0×10^{14} (48%/63%)
Measurement	⋯	7.9×10^{13} (38%/49%)

VI. DISCUSSION

Assuming short lens approximation and a homogeneous filled space charge cylinder, the measured focal length given by

$$\frac{1}{f}=\frac{r'}{r_0}=k^2l=\frac{n_e e}{4\varepsilon_0 U_B}l \tag{12}$$

is a function of the length l of the space charge cylinder and the space charge density $n_e e$. For the determination of the space charge density, the length of the space charge cloud is necessary.

TABLE II. Comparison of space charge particle densities gained by theory, simulation, and measurements for the second lens.

Lens 2	$n_{e,\max}[\mathrm{m}^{-3}]$	$\bar{n}_e[\mathrm{m}^{-3}]$
Radial enclosure	2.9×10^{14}	2.9×10^{14}
Longitudinal enclosure	2.3×10^{14}	2.3×10^{14}
Simulation	2.1×10^{14} (72%/90%)	1.4×10^{14} (49%/61%)
Measurement	⋯	1.4×10^{14} (49%/61%)

The length of the cloud can be assumed by the distance between the two grounded electrodes (106 mm). The measured focal length for the first lens is 0.366 m and for the second 0.22 m. For the first lens an average density of 7.9×10^{13} particles per cubic meter can be derived from the measurements. The maximum densities forecasted by theory and simulations for the first experiment are listed in Table I. The data show a local maximum degree of lens filling of 70% for the radial enclosure and more than 90% for the longitudinal trapping. The average degree of lens filling in the simulation is 48% and 63%, respectively. This is due to the reduced space charge densities in the peripheral of the cloud. The measurements show an average degree of lens filling of 38% and 49%. Therefore the measured average charge density is 79% of the value gained by the simulation.

For the second lens, an average density of 1.4×10^{14} particles per cubic meter can be derived from the measurements. The maximum density forecasted by theory and simulations for the second lens are listed in Table II. The data show again a local maximum degree of lens filling of 72% for the radial enclosure and more than 90% for the longitudinal trapping. The average degree of lens filling in the simulation was 49% and 61%, respectively. The measurements show an increased average degree of lens filling of 49% and 61% for the second lens, as predicted by the simulations.

[1] Westphal, Ann. Phys. **27**, 586 (1908).
[2] B. Johnson, J. Opt. Soc. Am. **6**, 701 (1922).
[3] B. Borries and E. Ruska, Z. Phys. **76**, 649 (1932).
[4] D. Gabor, Nature (London) **160**, 89 (1947).
[5] L. Brillouin, Phys. Rev. **67**, 260 (1945).
[6] J. Pozimski *et al*., HEDIM Annual Report 1997, GSI-98-09 (1998).
[7] R. M. Mobley, IEEE Trans. Nucl. Sci. **NS-26**, 3112 (1979).
[8] R. Booth and H. W. Levevre, Nucl. Instrum. Methods **151**, 143 (1978).
[9] J. A. Palkovic, "Measurements on a Gabor lens for neutralizing and focusing a 30 keV proton beam", Ph.D. thesis, University of Wisconsin, Madison, 1991.
[10] M. Reiser, Proc. PAC Conf. Chicago, 1989, p. 1744.
[11] J. Pozimski, P. Groß, R. Dölling, and H. Klein, Proc. LINAC Geneva, CERN 96-07, 1996, p. 80.
[12] J. Pozimski and O. Meusel, GrakoNews **1**, 20 (1999); electronic mail: grako@ikp.tu.darmstadt.de
[13] J. Pozimski and O. Meusel, HEDIM Annual Report 2002, GSI-2003-07, 2003.